Article:
Ding, Y., Olumayegun, O., Chai, Y. et al. (2022) Simulation, energy and exergy analysis of compressed air energy storage integrated with organic Rankine cycle and single effect absorption refrigeration for trigeneration application. Fuel, 317. 123291. ISSN: 0016-2361

https://doi.org/10.1016/j.fuel.2022.123291

Simulation, energy and exergy analysis of compressed air energy storage integrated with Organic Rankine Cycle and single effect absorption refrigeration for trigeneration application

Yuxing Ding[a], Olumide Olumayegun[a], Yue Chai[a], Yurong Liu[b], Meihong Wang[a]*

[a] Department of Chemical and Biological Engineering, The University of Sheffield, Mappin Street, Sheffield S1 3JD, UK

[b] Key Laboratory of Advanced Control and Optimization for Chemical Processes, Ministry of Education, East China University of Science and Technology, Shanghai 200237, China

Abstract

Compressed air energy storage (CAES) is increasingly investigated as a viable technology for balancing electricity supply and demand. The main purpose of CAES is to overcome the intermittent problem when renewable energy is introduced. However, the round-trip efficiency (RTE) of the CAES system commercially developed is still low (around 54%) and requires further improvement. This study proposed a novel combined cooling, heating and power (CCHP) system, which improves the RTE in two ways: (i) Organic Rankine Cycle (ORC), which recovers the waste heat and produces extra power; (ii) single effect absorption refrigeration, which delivers cooling capacity with further recovery of waste heat from the flue gas. Steady-state process simulation of the CAES system, ORC and single effect absorption refrigeration system was developed in Aspen Plus® software. The proposed system was evaluated through process, energy, and exergy analysis. The effect of various working parameters on the performance of the CCHP system was also analysed. The results indicated that under

design condition, the proposed CCHP system can produce about 206 MW electrical energy, 28 MW heating and 0.2 MW cooling capacity. The RTE of the proposed system (about 66%) showed an improvement of approximately 12% when compared with the CAES system commercially deployed. The overall exergy efficiency is about 51% and the total exergy destruction of the components of the system is 477 MW. The combustion chamber is responsible for more than half of the exergy destruction.

Keywords

Compressed air energy storage (CAES); Organic Rankine Cycle (ORC); Trigeneration; Combined cooling, heating and power (CCHP); Process simulation; Exergy analysis

Nomenclature

Q	Heat transfer (kW)
W	Work (kW)
T	temperature (°C)
h	Specific enthalpy (kJ/kg)
s	Specific entropy (kJ/kg K)
Com	Compressor
Tur	Turbine
Cave	Cavern

HX	Heat exchanger
Val	Valve
Cc	Combustion chamber
pum	Pump
OT	Organic turbine
Des	Desorber
orc-c	ORC in charging process
orc-d	ORC in discharging process
pum-c	pump in charging process
pum-d	ORC pump in discharging process
Evap	Evaporator

Abbreviations

CAES	Compressed air energy storage
RTE	Round trip efficiency
ORC	Organic Rankine Cycle
GHG	Greenhouse gas
IEA	International Energy Agency
PHS	Pumped hydro storage
SMES	Superconducting magnetic energy storage

CCHP	Combined cooling, heating and power
D-CAES	Diabetic compressed air energy storage
KC	Kalina Cycle
LiBr	Lithium bromide
PENG-ROB	Standard Peng-Robinson cubic equation of state
COP	Coefficient of performance
Abs	Absorber
Aftc	After-cooler
G	Generator
GHG	Greenhouse gas
HPC	High pressure compressor
Intc	Inter-cooler
LPC	Low pressure compressor
M	Motor
Rec	Recuperator
Reg	Regulating valve
SHX	Solution heat exchanger
RTE	Round-trip efficiency
V	Valve

38

39

40

41 # 1. Introduction

42 ## 1.1. Background

43 In recent decades, the consumption of fossil fuels has caused global environmental
44 problems, due to the production of greenhouse gases (GHG) (Chai et al., 2020; Meng
45 et al., 2019). Hence, renewable energy sources are being utilised to reduce the
46 dependency on fossil fuels and cut CO_2 emissions (Aneke and Wang, 2016). Renewable
47 energy has been growing significantly over the years. According to the 2020 world
48 renewable electricity statistics, released by the International Energy Agency (IEA), the
49 share of all renewables in electricity generation reached 27% (7486 TWh) in 2020 (IEA,
50 2020). However, the main problem with renewable energy is its intermittence,
51 especially for wind power and photovoltaics (Budt et al., 2016; Luo et al., 2015).
52 Furthermore, renewable energy production methods cannot be continuous, and the
53 output depends on geographic location and climate (Meng et al., 2019; Zhao et al.,
54 2016). Researchers have suggested energy storage technologies to solve the
55 intermittence problem (Sadreddini et al., 2018; Aneke and Wang, 2016). Such
56 technologies have numerous benefits, especially in peak shaving, black start, load
57 levelling, renewable integration, power quality improvement and energy arbitrage
58 (Meng et al., 2018; Aneke and Wang, 2016; Luo et al., 2015; Sioshansi et al., 2011;
59 Chen et al., 2009).

60 Many energy storage technologies have been commercialised or are still under research.
61 These include pumped hydro storage (PHS), compressed air energy storage (CAES),
62 batteries, fuel cells, flywheels, superconducting magnetic energy storage (SMES),

63 capacitors and supercapacitors (Letcher, 2020; Meng et al., 2018; Aneke and Wang,
64 2016; Luo et al., 2015; Kousksou et al., 2014; Chen et al., 2009). Among these energy
65 storage technologies, only PHS and CAES are suitable for large grid-scale (>100 MW)
66 systems due to their high energy capacity, high power rating, and long discharge time
67 (Letcher, 2020; Meng et al., 2018). However, PHS power plants require suitable
68 geographical conditions for the construction of reservoirs and dams, with a long
69 construction period and significant initial investment (Letcher, 2020; Meng et al., 2018;
70 Aneke and Wang, 2016; Chen et al., 2009). The huge benefits of CAES technology
71 include high reliability and round-trip efficiency (RTE), providing reserve power and
72 economic feasibility (Budt et al., 2016; Chen et al., 2009).
73 However, the RTE of the CAES system still needs further improvement. Combined
74 cooling, heating and power (CCHP) systems are among the most attractive and
75 promising solutions to reduce energy consumption (Mohammadi et al., 2017;
76 Sadreddini et al., 2018; Razmi et al., 2019). Most conventional CCHP systems are based
77 on gas-fired power plants, which cannot fully realise their energy-saving advantages
78 (Gao et al., 2015; Yan et al., 2018). The integration of CAES, Organic Rankine Cycle
79 (ORC) and a refrigeration system for CCHP application has many advantages: (i) it
80 generates three different products: cooling, heating and electricity; (ii) it improves the
81 efficiency of energy use; (iii) it reduces the emission of air pollutants (Mohammadi et
82 al., 2017; Sadreddini et al., 2018; Razmi et al., 2019).

83 1.2. Literature review

84 To date, there are two large-scale CAES plants in commercial operation. Diabatic
85 compressed air energy storage (D-CAES) is the primary type of CAES plant, and these
86 two CAES plants are of this type (Zhou et al., 2019; Budt et al., 2016). The first is the
87 Huntorf CAES plant, built in Germany and in operation since 1978. The Huntorf CAES

88 plant, with the RTE of 42%, could produce 290 MW electricity for a 2~3h discharging
89 duration (Meng et al., 2018; Chen et al., 2009; Crotogino et al., 2001). The second
90 CAES plant was built in McIntosh, Alabama, USA and has been in operation since 1991.
91 The McIntosh CAES plant could produce 110 MW of electricity for a 26h discharging
92 duration (Meng et al., 2018; Aneke and Wang, 2016; Budt et al., 2016; Luo et al., 2015;
93 Chen et al., 2009). However, the Huntorf CAES plant has unique benefits as it can be
94 operated as reserve power and black-start capacity (Radgen, 2008; Budt et al., 2016).
95 Many studies have focused on the investigation of the CAES system integrated with
96 renewable energy (wind and photovoltaic power) to overcome the intermittence
97 problem (Meng et al., 2019; Zhang et al., 2017; Krupke et al., 2016; Zhang et al., 2014;
98 Cavallo, 2007; Cazzaniga et al., 2017; Simpore et al., 2016; Arabkoohsar et al., 2015).
99 In addition, some researchers have focused on the investigation of the CAES integrated
100 with a waste heat recovery system (Meng et al., 2018; Mohammadi et al., 2017). The
101 ORC and Kalina Cycle (KC) could recover waste from a gas turbine exhaust in the
102 CAES system to improve the RTE (Meng et al., 2018; Quoilin et al., 2013). Furthermore,
103 Soltani et al. (2020) analysed and compared ORC and KC combined with CAES. Their
104 findings indicated that the highest RTE is achieved by the ORC-R290 cycle, with a 2.67%
105 increase. Additionally, the ORC has been demonstrated to have a low operating cost
106 and a long plant life, which is more commercially viable (Meng et al., 2018; Sadreddini
107 et al., 2018; Pinerez et al., 2021).
108 Recently, utilising the CAES system for the CCHP system has been receiving increased
109 attention (Mohammadi et al., 2017; Sadreddini et al., 2018; Razmi et al., 2019).
110 Additionally, He et al. (2015) performed model development and thermodynamic
111 analysis for CAES combined with a CCHP system. It was found that the proposed
112 system could minimise fuel consumption (29.4%) and maximise the exergy efficiency

(31.8%). Furthermore, Yao et al. (2016) developed a CCHP system based on a small-scale D-CAES system to investigate the dependence of the system's thermodynamic performance on the design variables. The results showed that the efficiency point of 51% is preferred for industrial applications. Yan et al. (2018) developed an active storing strategy for a novel CCHP system integrated with CAES, and the novel algorithm C-NSGA-II makes the model more accurate. The proposed methodology could be applied to future research on CCHP system optimisation. The results showed that the daily cost decreases by 4.45% to increase the environmental benefits. Souza et al. (2020) proposed a co-generation system using the ORC and an absorption refrigeration system through energy, exergy and exergoeconomic assessment. The results indicated that ORC-C allowed increases of 33.6% in power production and 34.5% in energy efficiency.

In addition, very few studies have focused on the CCHP system based on CAES, for a waste heat recovery system and cooling system. Mohammadi et al. (2017) proposed a CCHP system composed of CAES, ORC and an ammonia-water absorption refrigeration system. It was found that the CCHP system could achieve a RTE of 53.94% under the design condition. Sadreddini et al. (2018) developed a new cogeneration system composed of CAES, ORC and an ejector refrigeration system. The study used an optimisation process (genetic algorithm) with the aim being to find the optimal solution. The results showed that the RTE of the system increased by 5.7%, from 68% to 71.88%.

In this present study, a CCHP system comprising of CAES, ORC and a single-effect $LiBr/H_2O$ absorption system is proposed. A detailed process description of the CCHP system is given in Section 2. Furthermore, the CCHP system can be integrated with the renewable energy to overcome the intermittence problem. There are three points to increase the RTE of the CCHP system: (1) the use of a recuperator in the proposed

CCHP system, (2) the use of a multi-stage centrifugal compressor with six intercooled stages, (3) the use of ORC integrated with the CAES system.

1.3. Motivation

The new cogeneration system is composed of a CAES system, ORC and a single effect absorption refrigeration system. The CAES system is the potential technology for large-scale energy storage. The ORC can be integrated with the CAES system to recover the waste heat and improve the RTE during charging and discharging time. The hybrid system has all the advantages of energy storage technology and can produce three different commodities, namely power, cooling, and heating. The hybrid system is investigated and analysed through simulation and thermodynamic analysis to improve system performance in this work.

1.4. Aims and novel contributions

In this study, a high-efficiency cogeneration system, comprising a CAES system, ORC and a single effect absorption refrigeration system, is investigated. The aim of this study is to improve the RTE of the hybrid system. During the charging process, the ORC could recover waste heat from the multi-stage compressors. The heat source of the single-effect absorption refrigeration system is flue gas recovered from the low-pressure turbine. The proposed CCHP system has some advantages. Firstly, it can provide cooling, heating and power simultaneously, with high RTE. Secondly, it can be utilised as peak shaving. To achieve this aim, the following objectives have been identified:

- To develop steady-state models of CAES, ORC and single effect absorption refrigeration system in Aspen Plus®.
- Model validation of CAES, ORC, and single effect absorption refrigeration system.

- Energetic and exergetic performance evaluation of the integrated system.
- Sensitivity analysis of the system performance to study the effect of compressor inlet temperature, inter-cooler temperatures, ORC turbine inlet pressure and vapour generator temperature.

The novel contributions of this study include:

- A new CCHP system composed of CAES, ORC and a single effect absorption refrigeration system is proposed.
- A new scheme to improve the RTE is proposed for the CAES system.
- The process performance is analysed through energy and exergy analysis.
- Sensitivity analysis of different important parameters is undertaken.

2. System description

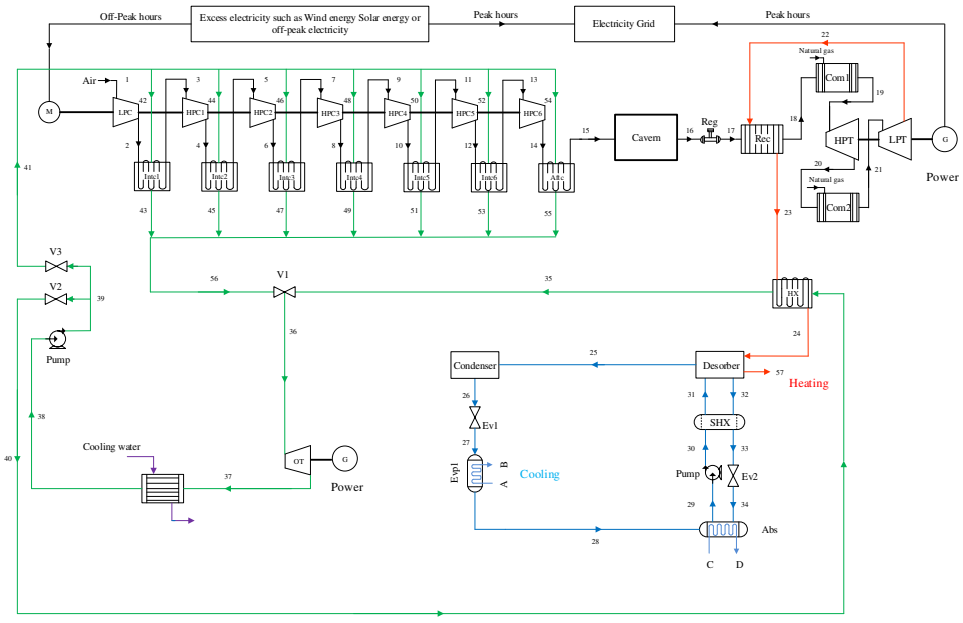

Figure 1. Schematic diagram of the proposed system

A schematic diagram of the newly proposed CCHP system is shown in Fig 1, consisting of a CAES system, an ORC and a single effect absorption refrigeration system. The

178 CCHP system itself is composed of two subsections, including charging and
179 discharging subsystems.
180 In the charging process, the multi-stage compressors compress air to a high pressure
181 and store it in the cavern, converting electrical energy into the internal energy of the air,
182 for storage during off-peak power consumption periods. The advantages of using multi-
183 stage compressors are improved efficiency, less moisture build-up and a smaller
184 footprint (Meng et al., 2018; McNevin and Harrison, 2017). An ORC is used to recover
185 low-grade waste heat from the multi-stage compressors, using inter-coolers and after-
186 coolers to improve the RTE (Meng et al., 2018; Quoilin et al., 2013). The ORC is
187 comprised of an evaporator, expander, condenser, pump and heat exchangers. Then, the
188 organic working fluid will be pumped into the evaporator to be heated and transformed
189 into evaporated liquid. Finally, the evaporated fluid passes into the expander to generate
190 more power (Meng et al., 2018; Wang et al., 2013).
191 In the discharging process, the high-pressure air is released from the cavern and heated
192 in the recuperator, by recovering the waste heat from the exhaust of the low-pressure
193 turbine. The fuel is then burnt in the combustion chamber by mixing with the preheated
194 air. The high-temperature and high-pressure gas enters the turbine where it is expanded
195 to generate electricity during peak electricity consumption (Budt et al., 2016; Zhou et
196 al., 2019). However, the low-pressure gas turbine still has some waste heat, one part is
197 used to drive the ORC turbine and the other to drive the desorber. The recovered waste
198 heat can further improve the round-trip efficiency of the CCHP system and generate
199 cooling capacity.
200 Single effect absorption refrigeration systems can be driven by waste flue gas from a
201 low-pressure gas turbine. The advantages of using a single effect absorption
202 refrigeration system integrated with an ORC include high economic efficiency and

being environmentally friendly (Misra et al., 2003; Gomri, 2009). The single-effect absorption refrigeration system consists of the desorber, condenser, evaporator, absorber, and solution heat exchanger. In this study, Lithium bromide (LiBr) is used as the absorbent and water is considered the refrigerant of the refrigeration cycle. The reason is that the refrigeration system has the characteristics of high economic efficiency, safety reliability, non-toxicity and the odourless LiBr solution (Chen et al., 2017; Misra et al., 2003). The working principle of a single effect absorption refrigeration system can be divided into two parts: One part is separated from the solution as cold agent water vapour, and the other becomes a concentrated lithium bromide solution. The separated water vapour is condensed into water by a condenser and then evaporated by an evaporator to absorb heat and produce cold before entering the absorber and mixing with the concentrated lithium bromide solution to form a dilute lithium bromide solution. Conversely, the concentrated lithium bromide solution in the generator, after heat exchanging with the dilute lithium bromide solution, enters the absorber through the throttle valve, where it combines with the refrigerant vapour and dilutes into a dilute solution. This solution passes through the solution pump and the solution heat exchanger before entering the generator. Through the working process, a cooling capacity is generated.

3. Model development and validation

Aspen Plus® is a general-purpose steady-state process simulation software. In this study, the CAES system, the single effect absorption refrigeration system and the ORC are developed and simulated by Aspen Plus® V12. Each subsystem has been validated separately because the proposed system is yet to be built.

3.1. CAES model development and validation

CAES can be divided into two parts: charging and discharging. To decide the round-trip performance, some system and component parameters need to be specified (Meng, 2019; Canepa et al., 2013). The following is a list of the steady-state simulation assumptions (Meng et al., 2018; Zhao, Dai and Wang, 2015; Mohammadi et al., 2017; Sadreddini et al., 2018):

1. The flow remains in a steady state condition over the entire length of the streamlines.
2. The assumed air content is 78 vol% nitrogen, 21 vol% oxygen, and 1 vol% Ar.
3. The isentropic efficiency of the compressors is 75%.
4. The isentropic efficiency of the turbines is 93%.
5. The mechanical efficiency of compressors and turbines is 100%.
6. Exergy ambient reference condition of 25°C and 1.01325 kPa.
7. The pressure in the combustion chamber is the same as the cavern outlet pressure (4.6 MPa).
8. The fuel of choice in combustion is natural gas, and its temperature is set to 32°C.
9. Pump mechanical efficiency of 80%.

The physical properties were calculated using the PENG-ROB (Standard Peng-Robinson cubic equation of state) method. The PENG-ROB method was developed by Peng and Robinson in 1976 (Meng et al., 2019; Liu et al., 2014), and was selected for the property calculation for the CAES model.

The different critical components of the CAES system were simulated with different blocks in Aspen Plus®, as summarised in Table 1.

250 **Table 1.** The different CAES components simulated in Aspen Plus®.

Components	Blocks
Compressors / Turbines	*Compr*
Inter-cooler / After-cooler	*Heater*
Pressure regulating valve	*Valve*
Recuperator	*HeatX*
Cavern	*Tank*
Combustors	*RGibbs*
Water pump	*Pump*

251

252 The Huntorf CAES plant data were collected from Meng (2019), Budt et al. (2016) and
253 Hoffein (1994) to validate the models. Figure 2 shows the flowsheet of the Huntorf
254 plant. Table 2 presents the key input process conditions and parameter values for
255 thermodynamic simulation in Aspen Plus®. Table 3 shows the results of the steady-state
256 simulation against the Huntorf CAES plant. The results show that the relative error is
257 less than 0.38%.

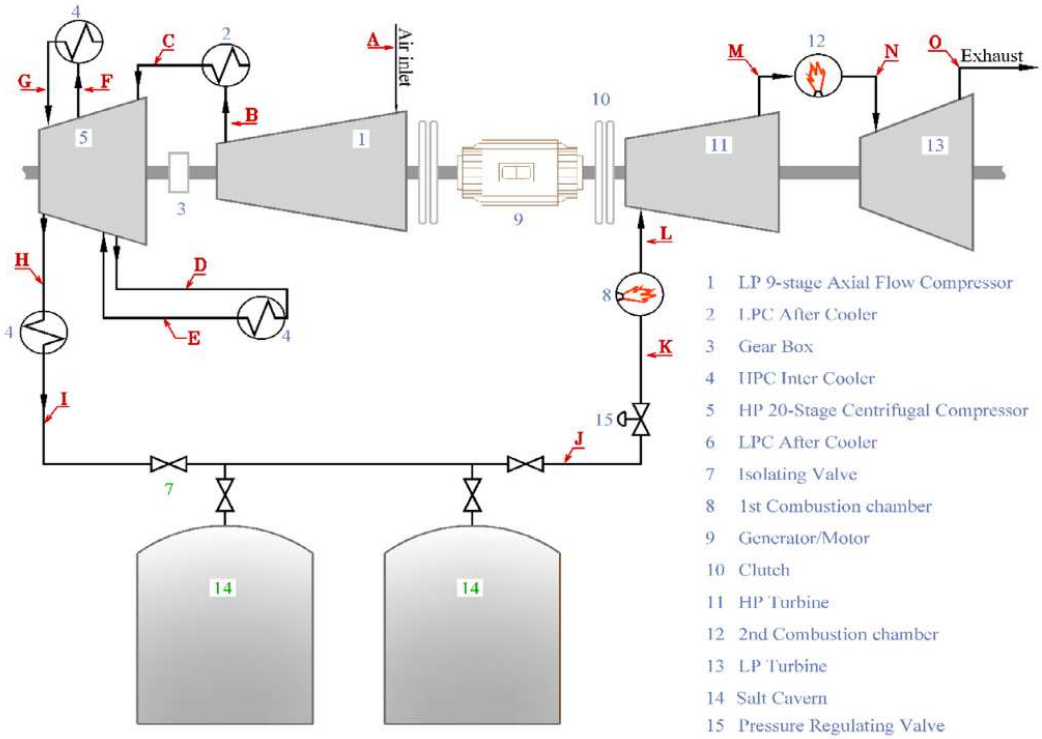

Figure 2. Schematic diagram of Huntorf CAES plant (Jafarizadeh et al., 2020)

Table 2. The critical operational parameters of Huntorf plant

Main Streams	Process	Parameters	Value
1	Charging	Rated air mass flow rate	108 kg/s
2	Charging	Rated power of compressor	60 MW
3	Charging	Inter-cooler outlet temperature	50°C
4	Charging	Inter-cooler outlet pressure	4.6-7.2 MPa
5	Charging	Operation time	8 h
6	Charging	Compressor stage	2
7	Charging	High pressure ratio	8
8	Charging	Low pressure ratio	6
9	Discharging	Rated power of turbine	290 MW
10	Discharging	Rated air mass flow rate	417 kg/s

11	Discharging	Inlet pressure of 1-stage turbine	4.2 MPa
12	Discharging	Inlet temperature of 1-stage turbine	550°C
13	Discharging	Inlet pressure of 2-stage turbine	1.13 MPa
14	Discharging	Inlet temperature of 2-stage turbine	825°C
15	Discharging	Operation time	2 h

261

262 **Table 3.** Model validation results (with Huntorf CAES plant)

Parameters	**Huntorf data**	**Simulation results**	**Relative errors (%)**
Compressors consumption (MW)	60	60.11	0.18
Rated power of turbine (MW)	290	291.11	0.38

263

264 As the data from the Huntorf plant is not sufficiently detailed, an additional model
265 comparison with Kakodkar (2018) was carried out. Table 4 shows the results of the
266 steady-state simulation compared with literature data from Kakodkar (2018).

267 **Table 4.** The critical operational parameters of Kakodkar (2018)

Parameters	**Literature Data**	**Simulation Results**	**Error (%)**
Inlet temperature of cavern (°C)	35	35	0
Outlet temperature of recuperator (°C)	642.6	642.35	0.03
Outlet temperature of combustor (°C)	712.67	712.53	0.01
Outlet pressure of turbine (MPa)	15	15	0
Outlet temperature of turbine (°C)	1562.56	1563.12	0.03

Outlet mass flow rate of cavern (kg/s)	400	400.85	0.21
Round-trip efficiency (%)	52.45	53	1.04
Compressors consumption (MW)	50	50.2	0.4
Rated power of turbine (MW)	167	167.78	0.46

268

269 3.2. ORC model development and validation

270 Figure 3 shows the main components of the ORC. The main working process comprises
271 four components: pump, evaporator, expander and condenser.

272 The pump is used to increase liquid pressure. The high-pressure liquid then enters the
273 evaporator where it is evaporated to form high pressure saturated vapour. The saturated
274 vapour then passes through the expander where it expands and drives a turbine to
275 generate electricity.

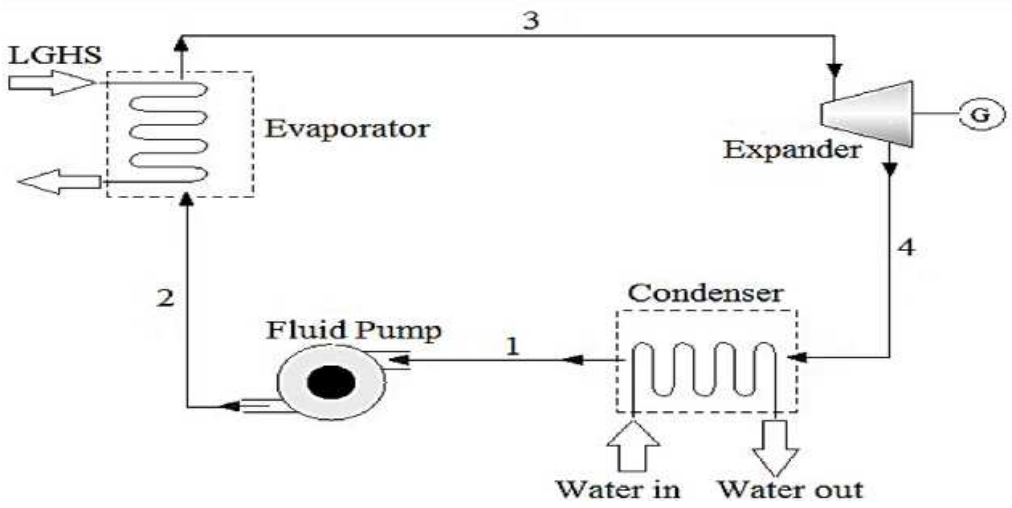

276

277 **Figure 3.** Schematic diagram of simple ORC (Kheiri and Ghaebi, 2016).

278 The main components of the ORC are simulated with different blocks in Aspen Plus®,
279 as summarised in Table 5.

280 **Table 5.** The different ORC components simulated in Aspen Plus®.

Components	Blocks
Evaporator/ Condenser	*HeatX*
Recuperator	*HeatX*
Pump	*Pump*
Expander	*Compr*
Pressure-regulating valve	*Value*

281

282 The validation data for the ORC model were obtained from Kanoglu and Bolatturk,
283 (2008) for the geothermal power plant in Reno, NV, USA. The organic working fluid
284 used is R600a (Iso-Butane), which is a widely used refrigerant. The parameters in Table
285 6 are the input process conditions and main operational parameters used in the ORC
286 model. Table 7 shows the simulation results, which are compared to the reference plant
287 data, for model validation. The relative errors are all less than 5%, and the simulation
288 results agreed with the reference plant data.

289 **Table 6.** The different ORC components simulated in Aspen Plus®

Main streams	Parameters	Value
1	Hot steam inlet flowrate (kg/s)	555.9
2	Hot steam inlet temperature (°C)	158
3	Working fluid flowrate (kg/s)	305.6
4	Cooling water inlet temperature(°C)	3
5	Cooling water inlet mass flowrate (kg/s)	1695.6
6	Turbine inlet / outlet pressure (bar)	32.5/4.1
6	Turbine isentropic efficiency	85%

7	Pump efficiency	92.5%
8	Recuperator efficiency	95%
9	Expander efficiency	80%

290

291 **Table 7.** Model validation results (in comparison with Reno geothermal power plant)

Parameters	**Reference plant data**	**Simulation results**	**Relative errors (%)**
Hot steam outlet temperature (°C)	128	128.7	0.54
Cooling water outlet temperature(°C)	11.7	11.4	2.56
Turbine heat transfer power (kW)	21,744	21,366	1.74
Condenser heat transfer power (kW)	141,271	137,484	2.68
Evaporator heat transfer power (kW)	160,929	156,746	2.60
Pump heat transfer power (kW)	2087	2049	1.82
Output power of Expander (kW)	16,396	15,999	2.42

292

3.3. Single effect absorption refrigeration system model development and validation

Figure 4 shows the main components of a single-effect absorption refrigeration system.It uses thermal energy as the driving heat source to drive the entire refrigeration cycle and thus produce the cooling capacity. In this single effect absorption refrigeration system, water is the refrigerant, and the lithium bromide solution is the absorbent. After continuous heating of the lithium bromide solution in the generator, part of it is separated from the solution as cold agent water vapour, while the other part becomes a concentrated lithium bromide solution. The separated water vapour is condensed into water by the condenser and then evaporated by the evaporator to absorb heat to produce the cooling capacity.

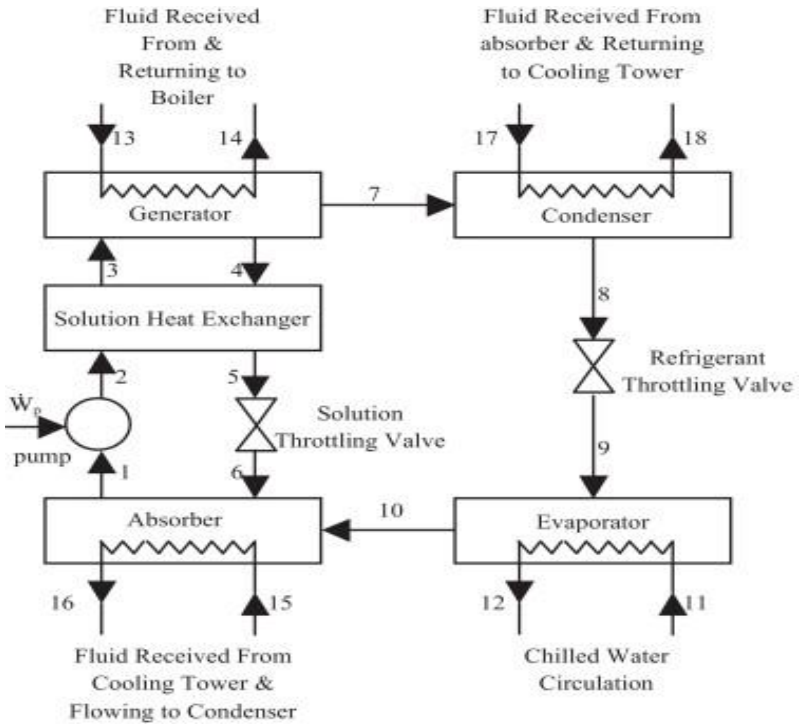

Figure 4. Schematic diagram of a single-effect LiBr/H_2O absorption system (Avanessian and Ameri, 2014).

Due to the LiBr solution being a strong electrolyte, the model physical property method is calculated using the ELECNRTL property method. For the absorption refrigeration

system in this paper, the cooling water is connected in series, entering the system from the absorber inlet, and leaving the system at the condenser outlet. The steady-state simulation assumptions for the single-effect LiBr/H_2O absorption system are given below:

(1) The generator's pressure is the same as the condenser, and the pressure of the absorber is the same as the evaporator.

(2) The thick solution of LiBr at the outlet of the generator and the diluted solution of LiBr at the outlet of the absorber are both saturated solutions.

(3) The pressure drops and heating loss of the piping and components are not considered.

(4) The amount of heat diffusion in the flow direction is ignored.

The components of a single-effect LiBr/H_2O absorption system are simulated with different blocks in Aspen Plus®, as summarised in Table 8 (Somers et al., 2011). Table 9 presents the key input process conditions and their values of a single-effect LiBr/H_2O absorption system for thermodynamic simulation in Aspen Plus®. Table 10 shows the simulation results compared with validation data from Herold et al., (2016).

Table 8. The different single-effect LiBr/H_2O absorption components were simulated in Aspen Plus®

Components	**Blocks**
Desorber	*Flash2, HeatX*
Solution heat exchanger	*HeatX*
Evaporator/ Condenser	*HeatX*
Absorber	*HeatX*

Pump	*Pump*
Throttling valve	*Valve2*

325 **Table 9.** The different single-effect LiBr/H_2O absorption components were simulated
326 in Aspen Plus®

Main streams	Parameters	Value
1	Desorber inlet temperature (°C)	100
2	Desorber inlet pressure (kPa)	7.406
3	Evaporator inlet pressure (kPa)	0.676
4	Evaporator cooling water inlet temperature (°C)	10
5	Condenser cooling water inlet temperature (°C)	25
6	Condenser inlet pressure (kPa)	7.406
7	Evaporator cooling water inlet flowrate (kg/s)	0.4
8	Absorber cooling water inlet flowrate (kg/s)	0.28
9	Absorber inlet flowrate (kg/s)	27.790
10	Evaporator inlet flowrate (kg/s)	23.480
11	Dilute solution mass fraction	57.5%
12	Thick solution mass fraction	61.5%

327

328 **Table 10.** Simulation results compared with literature data from Herold et al. (2016)

Parameters	Reference plant data	Simulation results	Relative errors (%)
Coefficient of performance	0.815	0.811	0.49

Concentration of dilute solution (%)	57.5	57.2	0.52
Concentration of thick solution (%)	61.5	61.37	0.21
Generator-Condenser heat transfer power (kW)	604.9	604.9	0
Absorber heat transfer power (kW)	583.6	583.6	0
Vapour compressor heat transfer power (kW)	514.3	514.3	0
Evaporator heat transfer power (kW)	493.1	493.1	0
Solution heat exchanger	66.72	66.59	0.19
Cooling capacity (kW)	10.00	10.00	0

329 3.4. Model development of CCHP system

330 The proposed CCHP system is comprised of three parts, namely the CAES, ORC and
331 single-effect LiBr/H_2O absorption system. To analyse the CCHP system, all models
332 have been developed and integrated successfully within a single flowsheet in Aspen
333 Plus® V12. For the CAES, the design data comes from the Columbia Hills CAES system
334 (McGrail et al., 2013). For the ORC and absorption system, the reasonable assumptions
335 were based on the output of the CAES system charging part, which ultimately ensured
336 that the model of the CCHP system would work well. The assumed input parameters'
337 design condition of the CCHP system is shown in Table 11.

338 **Table 11.** Design conditions of CCHP system (charging and discharging process)

Charging Process		
Parameter	Value	Unit
Ambient temperature	25	°C
Ambient pressure	1.013	bar
Pressure ratio of compressor	1.96177	-
Mass flow rate of compressor	353	kg/s
Compressor isentropic efficiency	75	%
Charging time	3	hour
Cavern inlet pressure	115.65	kg/s
Cavern outlet pressure	35.78	bar
Cavern inlet temperature	40.56	°C
ORC turbine inlet pressure	4	bar
Condenser pressure	4	bar
ORC turbine isentropic efficiency	80	%
ORC pump isentropic efficiency	80	%
Discharging Process		
Discharging time	6	hour
Inlet pressure of high-pressure turbine	34.40	bar
Turbine isentropic efficiency	93	%
Inlet pressure of low-pressure turbine	17.93	bar

Fuel inlet pressure of combustor 1	44.82	bar
Fuel inlet pressure of combustor 2	24.13	bar
Fuel inlet temperature of combustor 1	32.22	°C
Fuel inlet temperature of combustor 2	32.22	°C
Heat duty of recuperator	105.51	kW
ORC turbine inlet pressure	19.85	bar
Condenser pressure	4	bar
ORC turbine isentropic efficiency	80	%
ORC pump isentropic efficiency	80	%
Outlet temperature of Desorber	40.2	°C
Cooling system pump isentropic efficiency	85	%
Outlet temperature of Solution heat exchange	53.5	°C
Outlet pressure of Solution heat exchange	0.07461	bar

339

340 4. Thermodynamic analysis

341 4.1. Exergy analysis

342 Exergy is defined as the maximum shaft work that a system can perform in a specified
343 reference environment. Exergy analysis is a thermodynamic analysis technique resulted
344 from the second law of thermodynamics, which indicates exergy destruction.

345 The general exergy balance of a quantity can be calculated by:

346 $$Exergy\ Input + Exergy\ Generation - Exergy\ Outpt - Exergy\ Consuption = Exergy\ Accumulation \quad (1)$$

347 The exergy of work and heat can be expressed as (Mohammadi et al., 2017;

348 Sadreddini et al., 2018):

349 $$\dot{E}_x{}^{Q} = \left(1 - \frac{T_0}{T_i}\right)\dot{Q}_i \quad (2)$$

350 $$\dot{E}_x{}^{w} = \dot{W} \quad (3)$$

351 Where $\dot{E}_x{}^{Q}$ and $\dot{E}_x{}^{w}$ are exergy associated with heat and work; T_0 is the ambient

352 temperature and T_i is the temperature of the heat transfer. The exergy of the stream can

353 be divided into two parts, namely physical and chemical. The physical exergy is defined

354 as:

355 $$ex_{ph} = (h_i - h_0) - T_0(s_i - s_0) \quad (4)$$

356 Where, h_i is enthalpy, h_0 is enthalpy at the reference state, s_i and s_0 are specific

357 entropy, which related to different streams. The entropy term $(s_i - s_0)$ is defined as:

358 $$s_i - s_0 = C_{avg} ln \frac{T_i}{T_0} \quad (5)$$

359 Where C_{avg} is the average specific heat capacity of the substance.

360 The chemical exergy is defined as:

361 $$ex_{ch} = \sum_{i=1}^{N} y_i ex_i^{ch} + RT_0 \left(\sum_{i=1}^{N} y_i In(y_i)\right) \quad (6)$$

362 The ex is the sum of physical and chemical exergy, which can be calculated by the

363 following equation:

364 $$ex = ex_{ph} + ex_{ch} \quad (7)$$

365 Based on the above equations, exergy balance could be calculated as:

366 $$\dot{\mathrm{E}}_x{}^{Q} + \sum \dot{\mathrm{E}}x_{in} = \sum \dot{\mathrm{E}}x_{out} + \dot{\mathrm{E}}_x{}^{\mathrm{w}} + \dot{\mathrm{E}}_x{}^{D} \quad (8)$$

367 Where the $\dot{\mathrm{E}}_x{}^{D}$ is the exergy destruction of the component. Total exergy destruction

368 can be defined as:

369 $$\dot{\mathrm{E}}x_{total}^{D} = \mathrm{sum}\left(\dot{\mathrm{E}}_x{}^{D}\right) \quad (9)$$

370 Table 12 shows the exergy destruction and exergy efficiency equations used for the

371 calculation of exergy destruction and exergy efficiency of each key component.

372 **Table 12.** Exergy destruction of each component (Zhao et al., 2015; Mohammadi et

373 al., 2017; Sadreddini et al., 2018)

System component	Exergy destruction	Exergy efficiency
Compressor	$\dot{\mathrm{E}}x_{Com}^{D} = \dot{\mathrm{E}}x_{in} - \dot{\mathrm{E}}x_{out} + \dot{W}_{com}$	$\Psi_{\mathrm{Com}} = \frac{\dot{\mathrm{E}}x_{out} - \dot{\mathrm{E}}x_{in}}{\dot{W}_{Com}} \times 100$
Turbine	$\dot{\mathrm{E}}x_{Tur}^{D} = \dot{\mathrm{E}}x_{in} - \dot{\mathrm{E}}x_{out} - \dot{W}_{Tur}$	$\Psi_{\mathrm{Tur}} = \frac{\dot{W}_{Tur}}{\dot{\mathrm{E}}x_{in} - \dot{\mathrm{E}}x_{out}} \times 100$
Cavern	$\dot{\mathrm{E}}x_{Cave}^{D} = \dot{\mathrm{E}}x_{in} - \dot{\mathrm{E}}x_{out}$	$\Psi_{\mathrm{Cave}} = 1 - \frac{\dot{\mathrm{E}}x_{Cave}^{D}}{\dot{\mathrm{E}}x_{in}} \times 100$
Heat exchanger (Condenser, Evaporator, Intercoolers, Aftercooler and Recuperator)	$\dot{\mathrm{E}}x_{HX}^{D} = \sum \dot{\mathrm{E}}x_{in} - \sum \dot{\mathrm{E}}x_{out}$	$\Psi_{\mathrm{HX}} = \frac{(\dot{\mathrm{E}}x_{out} - \dot{\mathrm{E}}x_{in})_{cold}}{(\dot{\mathrm{E}}x_{in} - \dot{\mathrm{E}}x_{out})_{hot}} \times 100$

Value	$\dot{E}x_{Val}^{D} = \dot{E}x_{in} - \dot{E}x_{out}$	$\Psi_{\text{Valve}} = \frac{\dot{E}x_{in}}{\dot{E}x_{out}} \times 100$
Combustion chamber	$\dot{E}x_{Cc}^{D} = \dot{E}x_{in} - \dot{E}x_{fuel} - \dot{E}x_{out}$	$\Psi_{\text{Cc}} = \frac{\dot{E}x_{out} - \dot{E}x_{in}}{\dot{E}x_{fuel}} \times 100$
Pump	$\dot{E}x_{pum}^{D} = \dot{E}x_{in} - \dot{E}x_{out} + \dot{W}_{pum}$	$\Psi_{pum} = \frac{\dot{E}x_{out} - \dot{E}x_{in}}{\dot{W}_{com}} \times 100$
ORC turbine	$\dot{E}x_{OT}^{D} = \dot{E}x_{in} - \dot{E}x_{out} - \dot{W}_{OT}$	$\Psi_{\text{OT}} = \frac{\dot{W}_{OT}}{\dot{E}x_{in} - \dot{E}x_{out}} \times 100$
Desorber	$\dot{E}x_{Des}^{D} = \dot{E}x_{in} - \dot{E}x_{out} + \dot{W}_{VG}$	$\Psi_{Des} = \frac{\dot{E}x_{out} - \dot{E}x_{in}}{\dot{W}_{com}} \times 100$

374

375 4.2. Performance criteria

376 The performance criteria of D-CAES systems are different from those of conventional
377 power plants due to the charging process and the discharging process at different time
378 (as explained in Section 2). Another reason is that the first law efficiency cannot be
379 used to describe the CAES system. During the charging process, only the electrical
380 energy is used for the compressors work. The natural gas is combusted to heat
381 compressed air driving the turbine during the discharging process. Some waste heat in
382 the gas turbine is recovered by the ORC and single-effect LiBr/H_2O absorption system.
383 RTE is defined as the ratio of total energy output (comprising generated electricity of
384 the gas turbine and cooling energy) to the total energy input to the CAES system (Meng
385 et al., 2018; Zhaoet al., 2015):

386 $$\text{RTE}_{CAES} = \frac{W_{Tur}}{E_{fuel} + W_{Com}} \quad (10)$$

Where W_{Tur} is the output power of Turbine (kWh); W_{Com} is the electrical energy taken from the grid for driving the compressors (kWh); E_{fuel} is the thermal energy of fuel consumed (kWh). Based on Eq. (10), the RTE of the CCHP system could be described as:

$$\mathrm{RTE}_{CCHP} = \frac{W_{Tur} + W_{orc-c} + W_{orc-d} + W_{cooling}}{E_{fuel} + W_{Com} + W_{ORC,pum-c} + W_{ORC,pum-d} + W_{LiBr,pum}} \quad (11)$$

Where W_{orc-c} is the output power of the ORC in the charging process (kWh); W_{orc-d} is the output power of the ORC in the discharging process (kWh); $W_{cooling}$ is the output power of the single-effect LiBr/H_2O absorption system. $W_{ORC,pum-c}$ is the power consumption of the ORC pump in the charging process; $W_{ORC,pum-d}$ is the power consumption of the ORC pump in the discharging process; $W_{LiBr,pum}$ is the power consumption of the pump in the single-effect LiBr/H_2O absorption system.

For the CCHP system, the exergy destruction can be described as the difference between the total exergy flows into and out of the system minus the exergy accumulation in the system, which can be defined as:

$$\dot{\mathrm{E}}x^{D}_{total} = \mathrm{sum}\left(\dot{\mathrm{E}}x^{\mathrm{D}}\right) \quad (12)$$

Furthermore, the coefficient of performance (COP) is a ratio of useful cooling provided to work (energy) required that is used for the single-effect LiBr/H_2O absorption system, which can be defined as:

$$\mathrm{COP} = \frac{\mathrm{Q}}{\mathrm{W}} = \frac{\dot{\mathrm{Q}}_{\mathrm{Evap}}}{\dot{\mathrm{W}}_{\mathrm{Cooling}} + \dot{\mathrm{Q}}_{\mathrm{Des}}} \quad (13)$$

5. Results and discussion

The results of the proposed CCHP system analysis are given in this section.

5.1. Thermodynamic analysis

Table 13 lists the thermodynamic properties of each stream of the proposed CCHP system. The following assumptions are used for the analysis of the proposed CCHP system (Meng et al., 2018):

- The ambient reference temperature and pressure are 25℃ and 1.01325 kPa.
- All the cycles are at steady-state.
- The pressure drop, kinematic and potential energy of all components are ignored.
- Pure methane is used as the fuel in the combustion of the CAES discharging process.
- The outlet streams of the condenser are assumed to be saturated liquid.

Table 13. Thermodynamic properties of proposed CCHP system (charging and discharging process)

Charging process						
Steam Number	**Working Fluid**	**P [bar]**	**T [℃]**	**h [kJ/kg]**	**m [kg/s]**	**s [kJ/kg K]**
1	Air	1.013	25.00	-0.235	353.00	0.162
2	Air	1.987	109.06	84.504	353.00	0.219
3	Air	1.987	40.12	14.791	353.00	0.018
4	Air	3.898	129.01	103.819	353.00	0.075
5	Air	3.898	39.65	13.917	353.00	-0.178
6	Air	7.648	127.73	102.791	353.00	-0.121
7	Air	7.648	40.43	13.936	353.00	-0.371
8	Air	15.003	128.75	103.004	353.00	-0.314
9	Air	15.003	40.03	12.023	353.00	-0.569

10	Air	29.434	128.27	100.937	353.00	-0.513
11	Air	29.434	39.90	9.010	353.00	-0.771
12	Air	57.742	128.08	97.896	353.00	-0.715
13	Air	57.742	39.93	3.724	353.00	-0.980
14	Air	113.278	127.86	92.972	353.00	-0.923
15	Air	113.278	39.76	-5.453	353.00	-1.200
36	R600a	19.853	100.00	-2225.935	528.00	-6.666
37	R600a	4.000	52.16	-2278.147	528.00	-6.625
38	R600a	4.000	29.33	-2645.5457	528.00	-7.835
39	R600a	10.860	29.81	-2643.972	528.00	-7.834
41	R600a	19.853	29.81	-2643.972	528.00	-7.834
42	R600a	19.853	30.00	-2643.032	59.00	-7.837
43	R600a	19.853	100.00	-2225.935	59.00	-6.666
44	R600a	19.853	29.81	-2643.510	76.00	-7.838
45	R600a	19.853	100.00	-2225.935	76.00	-6.666
46	R600a	19.853	30.000	-2643.032	75.20	-7.837
47	R600a	19.853	100.00	-2225.935	75.20	-6.666
48	R600a	19.853	30.00	-2643.032	77.00	-7.837
49	R600a	19.853	100.00	-2225.935	77.00	-6.666
50	R600a	19.853	30.00	-2643.031	77.80	-7.836
51	R600a	19.853	100.00	-2225.935	77.80	-6.666
52	R600a	19.853	30.00	-2643.031	79.70	-7.836
53	R600a	19.853	100.00	-2225.935	79.70	-6.666
54	R600a	19.853	30.00	-2643.031	83.30	-7.836

55	R600a	19.853	100.00	-2225.935	83.30	-6.666
56	R600a	19.853	100.00	-2225.935	528.00	-6.666
57	Flue gas	1.03	94.21	-1237.250	193.63	0.318
Discharging process						
Steam Number	**Working Fluid**	**P [bar]**	**T [°C]**	**h [kJ/kg]**	**m [kg/s]**	**s [kJ/kg K]**
17	Air	35.780	40.56	8.605	189.00	-0.853
18	Air	35.780	561.24	567.377	189.00	0.191
19	Flue gas	34.400	676.67	689.262	189.53	0.349
20	Flue gas	18.270	545.07	538.902	189.53	0.363
21	Flue gas	17.930	1331.67	1444.571	193.64	1.166
22	Flue gas	1.030	600.61	528.478	193.64	1.247
23	Flue gas	1.030	115.56	-16.910	193.64	0.344
24	Flue gas	1.030	95.68	-37.909	193.64	0.289
25	Water	0.075	78.40	-13332.897	0.17	-0.950
26	Water	0.075	40.20	-15812.315	0.17	-8.849
27	Water	0.007	1.23	-15812.315	0.17	-8.810
28	Water	0.007	1.30	-13477.120	0.17	-0.305
29	LiBr-H_2O	0.007	32.70	-9919.965	1.00	-6.925
30	LiBr-H_2O	0.075	358.44	-9919.939	1.00	-6.358
31	LiBr-H_2O	0.075	50.48	-10251.041	1.00	-8.009

32	LiBr-H_2O	0.075	47.42	-9888.558	0.83	-10.280
33	LiBr-H_2O	0.075	53.30	-9491.444	0.83	-8.899
34	LiBr-H_2O	0.007	12.84	-9491.444	0.83	-9.815
35	R600a	19.853	100.00	-2225.935	10.00	-6.666
36	R600a	19.853	100.00	-2225.935	10.00	-6.666
37	R600a	4.000	52.16	-2278.147	10.00	-6.626
38	R600a	4.000	29.33	-2634.455	10.00	-7.811
39	R600a	19.853	30.62	-2630.819	10.00	-7.800
40	R600a	19.853	30.62	-2630.819	10.00	-7.800

Table 14 shows the main results of the CCHP system based on the equations and the data in Table 12. From Table 14, the charging time requires 8 hours to fill the cavern, and the discharging time requires 6 hours. This is because the discharging process of the CAES system needs to be performed during peak hours, which aims to maximise the revenue. During the charging process, 218421.63 kW power of electricity is consumed by the multi-stage compressors. The inter-cooler and after-cooler captured 220263.22 kW of heat. During the charging process, this captured heat is used to drive the ORC turbine. During the discharging process, the flue gas from the turbine still has some waste heat, which can be recovered by the ORC turbine to drive the desorber for the cooling system. The ORC and cooling system can recover low-grade heat and improve the RTE of the CCHP system. Moreover, the (high-pressure and low-pressure) turbines and ORC turbine each have a capacity of 233977.36 kW. The compressed air

reaches a pressure of 113.28 bar before entering the cavern, with an inlet mass flow rate of 353 kg/s. Since the charging process takes place during off-peak hours when electricity prices are low, this will vastly improve the system's economy value. The single-effect absorption refrigeration system can provide 245.45 kW of cooling capacity and the COP of the cooling system is 0.74. The COP of refrigeration systems is affected by various factors, including the inlet temperature of the heating source, the inlet temperature of the cooling water, and the outlet temperature of the refrigerant water (to be discussed in the following section). The addition of the ORC and refrigeration system allows the CCHP system to achieve a RTE of 66.35%, approximately a 23% improvement over the D-CAES system alone.

Table 14. Performance indicators of the CCHP system (Charging and discharging processes)

Charging process		
Parameter	**Value**	**Unit**
Charging time	3	Hour
$\dot{W}_{Com1}$	29913.29	kW
$\dot{W}_{Com2}$	31426.87	kW
$\dot{W}_{Com3}$	31372.62	kW
$\dot{W}_{Com4}$	31441.04	kW
$\dot{W}_{Com5}$	31386.49	kW
$\dot{W}_{Com6}$	31376.67	kW
$\dot{W}_{Com7}$	31504.65	kW
$\dot{W}_{comp,total}$	218421.63	kW

$\dot{E}_{comp,total}$	1747373.04	kWh
$\dot{Q}_{Intc1}$	24608.68	kW
$\dot{Q}_{Intc2}$	31735.71	kW
$\dot{Q}_{Intc3}$	31365.64	kW
$\dot{Q}_{Intc4}$	32116.41	kW
$\dot{Q}_{Intc5}$	32450.09	kW
$\dot{Q}_{Intc6}$	33242.57	kW
$\dot{Q}_{Aftc}$	34744.119	kW
$\dot{W}_{OT}$	27567.82	kW
$\dot{Q}_{Condenser}$	193986.41	kW
$\dot{W}_{ORC,pump}$	830.79	kW
Discharging process		
Parameter	**Value**	**Unit**
Discharging time	6	Hour
$\dot{W}_{HPT}$	28497.17	kW
$\dot{W}_{LPT}$	177390.27	kW
$\dot{Q}_{Com1}$	25874.17	kW
$\dot{Q}_{Com2}$	196809.55	kW
$\dot{Q}_{Rec}$	105607.815	kW
$\dot{Q}_{HX}$	4066.25	kW
$\dot{W}_{OT}$	522.12	kW
$\dot{Q}_{Condenser}$	3563.08	kW
$\dot{W}_{ORC,pump}$	36.36	kW

$\dot{Q}_{Desorber}$	330.72	kW
$\dot{Q}_{Condenser}$	260.63	kW
$\dot{Q}_{Evap}$	245.47	kW
$\dot{Q}_{Absorb}$	274.20	kW
$\dot{W}_{Cooling,pump}$	0.005	kW
$\dot{Q}_{SHX}$	134.91	kW
For whole process		
COP	0.74	—
E_{x-CCHP}	51.21	%
RTE	66.35	%

Figure 5 shows the results of the exergy analysis for the proposed CCHP system, based on the design conditions. From the results of exergy analysis, it can be seen that the highest exergy destruction (160635 kW) belongs to the combustion chamber. This is because the combustion process occurs in the combustor, and the combustor's irreversibility results in the highest level of exergy destruction. The use of fuels with a simple molecular structure containing oxygen molecules will reduce exergy destruction. Additionally, a recuperator can be used to preheat the air and fuel before introducing them into the combustion chamber, which is another effective way to prevent fire damage in the chamber. The second highest exergy destruction occurred at cavern 83716 kW, the third and fourth at the valve and recuperator, respectively. This is due to the significant temperature difference between the hot and cold flow entering these components.

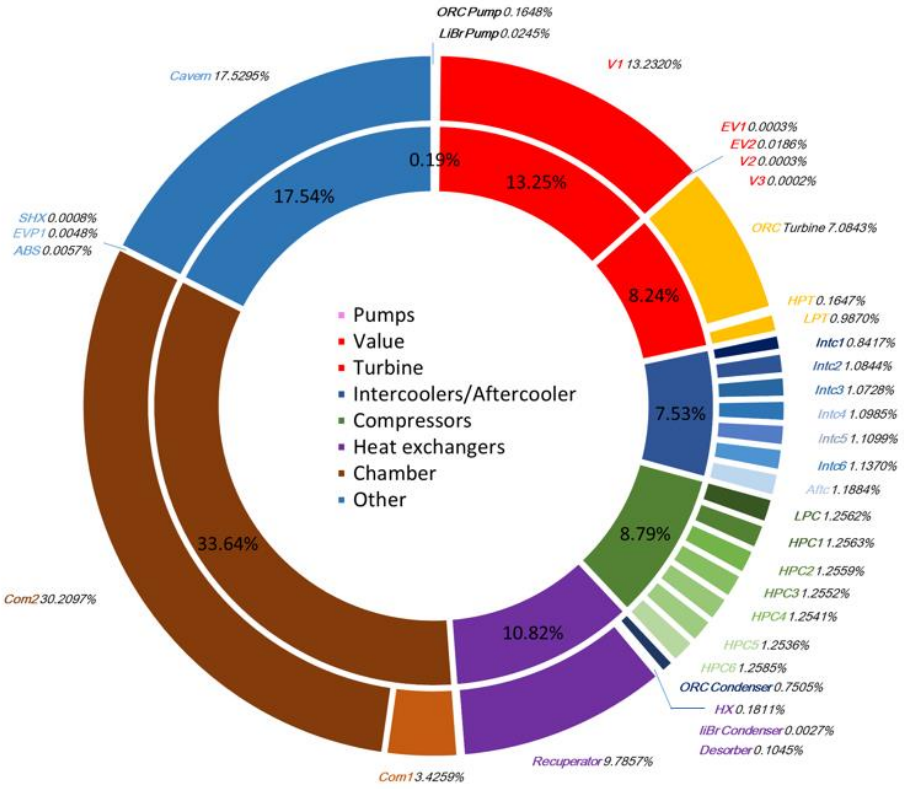

458

459 **Figure 5.** Exergy destruction of all components

460

461 5.2. Parametric analysis

462 The effect of the system's most critical parameters on performance is investigated in
463 this section by altering specific parameters while maintaining others constantly. The
464 effect of individual change in the inlet temperature of the compressor, the inlet pressure
465 of the ORC turbine, different working fluids for the ORC, the inlet temperature of
466 combustion chamber one and the inlet mass flow rate of the pump in the cooling system
467 on the performance of the proposed CCHP system are conducted.

5.2.1 Inlet temperature of the compressor

Figure 6 illustrates the effect of the compressor's inlet temperature variation on the CCHP system's performance. The higher inlet temperature of the compressor means a higher power output of multi-stage compressors. As the compressor's inlet air temperature increases, the exergy destruction of the CCHP system gradually decreases. When the inlet air temperature entering the compressor rises, the compressor needs less power output to work, which means a drop in overall compressor output. Based on Eq. (15), it will improve the RTE of CCHP system. It should be noted that the higher inlet temperature of the compressor leads to the higher exergy destruction. The main reason is that the variation of inlet temperature of the compressor only affects the charging process, whilst the chemical dissipation of the fuel and the output work of the gas turbine remains constant.

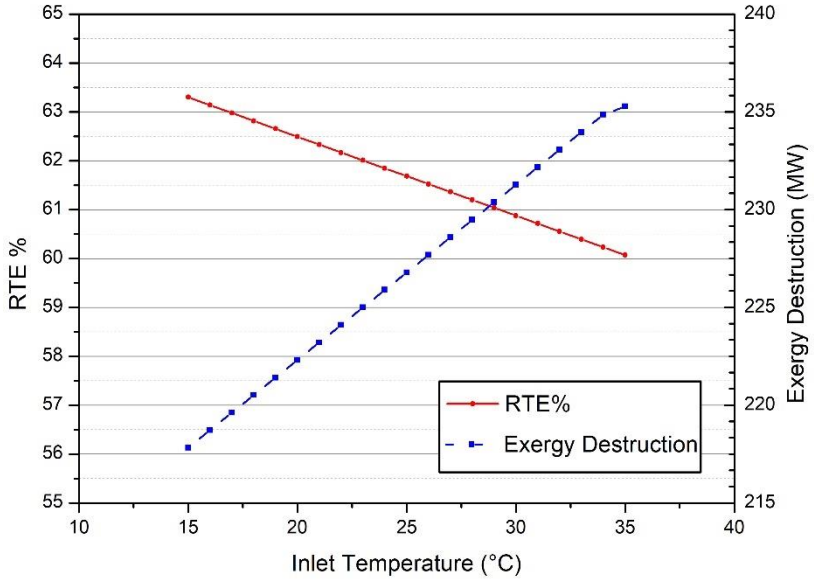

Figure 6. Effect of compressor inlet temperature variation on CCHP?? system performance

483 5.2.2 Inlet pressure of the ORC turbine

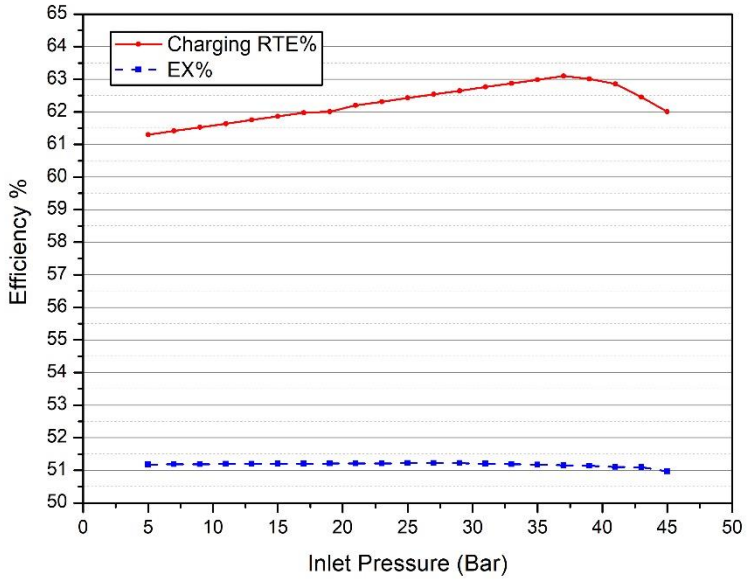

484

485 **Figure 7 (a).** Effect of inlet pressure of the ORC turbine on CCHP?? system

486 performance (charging process)

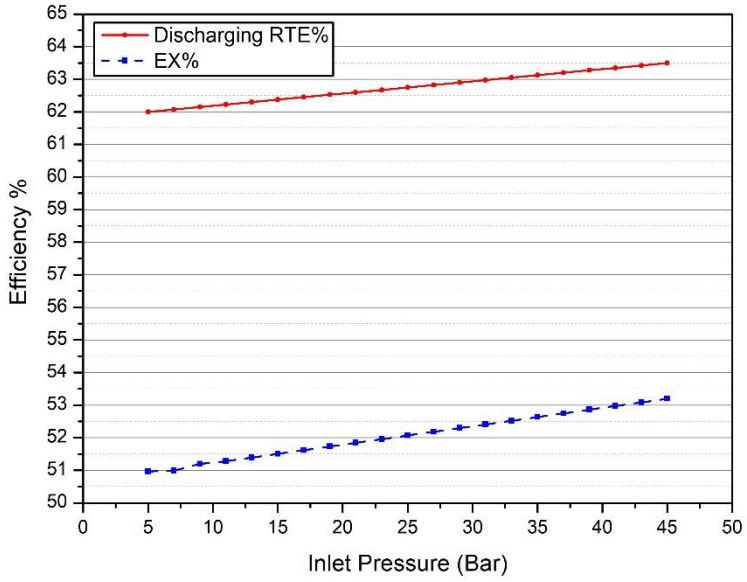

487

Figure 7 (b). Effect of inlet pressure of the ORC turbine on system performance (discharging process)

Figure 7 shows the effect of the inlet pressure of the ORC turbine on total exergy destruction and the RTE during (a) charging and (b) discharging processes. An increase in the inlet pressure leads to the increase of the ORC power output. The results show that an optimum inlet pressure exists for the ORC turbine, at which the power generated, and the subsequent cooling and heating capacity are maximised. The results show that the optimal operating point of inlet pressure during the charging process is around 35 bar. Additionally, both the RTE and the exergy efficiency of the system continue to grow with the growth of the inlet pressure during the discharging process. When the inlet pressure of the ORC turbine is at 35 bar, the proposed CCHP system could achieve the highest RTE (66.3%).

5.2.3 Different working fluids for ORC

The selection of organic working fluids for the ORC to achieve the maximum utilisation of waste heat is important. Therefore, the performance of different working fluids operating in specific regions is analysed. Figure 8 shows that using different working fluids has positive effects on RTE of the integrated system. In this proposed CAES system, due to the use of multi-stage compressors and setting the 3 hours charging time and 6 hours discharging time, the RTE of CAES only can reach up to 62.04%. This is a very significant improvement compared to the RTE (42%) of the Huntorf CAES plant. The results show that the RTE of the CCHP system increases by 4.11–5.56%.

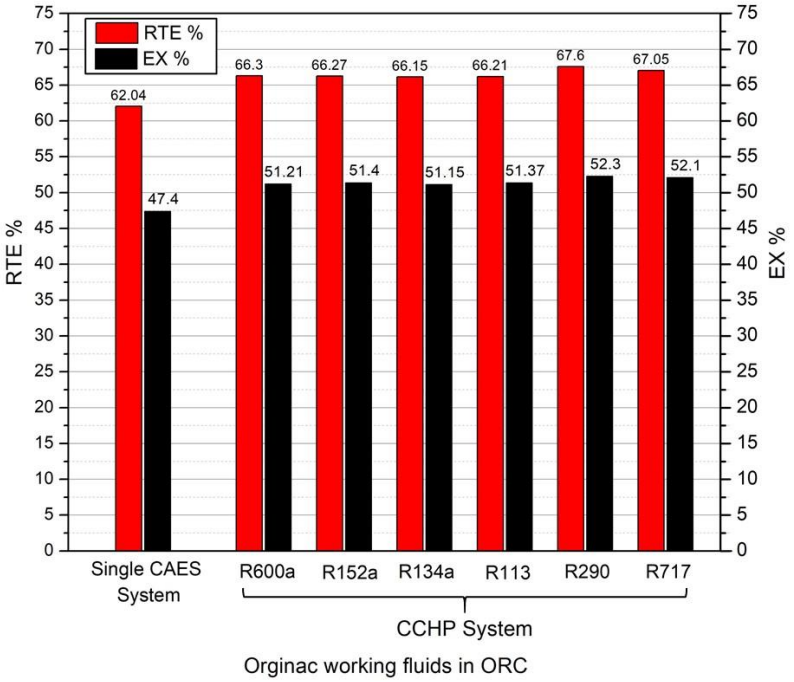

509

510 **Figure 8.** Effect of different working fluids of the ORC on system performance

511 5.2.4 Inlet temperature of combustion chamber 1

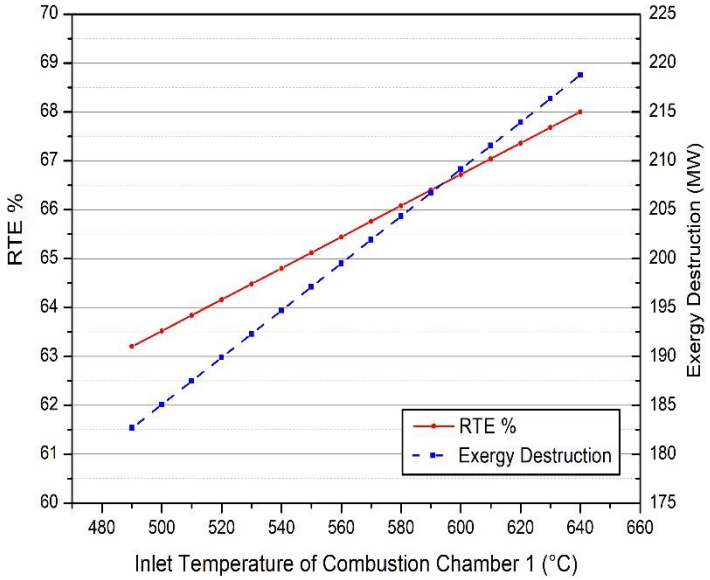

512

513 **Figure 9.** Effect of inlet temperature of combustion chamber 1 on system
514 performance

515

516 Figure 9 shows the effect of combustion chamber 1's inlet temperature on the system
517 performance. The results show that a higher inlet temperature implies higher gas turbine
518 power output. At the same time, it leads to a higher turbine outlet temperature, which
519 increases the power output generated in the ORC turbine as well. The cooling capacity
520 produced in the single effect absorption refrigeration system also increases due to the
521 higher generated heating from the flue gas.

522 5.2.5 Inlet mass flow rate of pump in single effect absorption refrigeration system

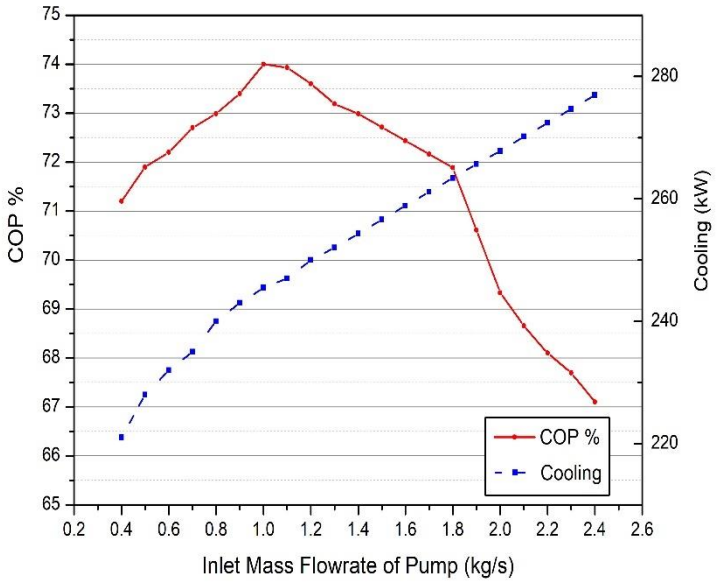

523

524 **Figure 10.** Effect of inlet mass flow rate of pump on system performance

525 Figure 10 shows the effect of the inlet mass flow rate of the pump on system
526 performance. Since the single effect absorption refrigeration system is located

downstream of the ORC, any change in its parameters does not have an effect on the ORC. The overall cooling capacity of the single effect absorption refrigeration system is not very large (245.45 kW) because the heating source comes from flue gas. From the results, it can be seen that the COP efficiency reaches a maximum of 74% at a mass flow rate of pump of 1 kg/s.

6. Conclusion

This study has proposed a new CCHP system comprised of a D-CAES system, ORC and a single effect absorption refrigeration system. The proposed CCHP system can produce power, heating and cooling. A comprehensive thermodynamic analysis of a CCHP system was applied to the system to analyse its performance. The main findings are summarised as follows: (a) The RTE of the proposed CCHP system has been improved by approximately 12% when compared with the McIntosh CAES plant (54%). Under the design condition, the RTE and overall exergy efficiency of the system are 66.35% and 51.21%, respectively. (b) At design conditions, the proposed CCHP system can produce 206 MW electrical energy, 28 MW heating and 0.2 MW cooling capacity, and the COP of the single effect absorption refrigeration system is 0.74. (c) Total exergy destruction of the CCHP system is equal to 478 MW, in which the combustion chamber is responsible for more than half of it. After the combustion chamber, the cavern, and recuperator have the highest value of exergy destruction. (d) R290 (Propane) as the ORC working fluid is the most suitable working fluid with the best performance. (e) Of all the parameters considered, the inlet temperature of the compressor, the inlet temperature of the combustion chamber and the inlet pressure of the ORC turbine are the most critical parameters, which can significantly improve the RTE and overall exergy efficiency. However, the proposed CCHP system has not been commercially

deployed. Further opportunities are emphasised: (1) Economic evaluation (2) Optimization to find the optimal operating conditions that maximize RTE. This research is expected to provide guidance for commercial deployment of CAES.

References

Aneke, M. and Wang, M., 2016. Energy storage technologies and real-life applications–A state of the art review. Applied Energy, 179, pp.350-377.

Arabkoohsar, A., Machado, L., Farzaneh-Gord, M. and Koury, R.N.N., 2015. Thermo-economic analysis and sizing of a PV plant equipped with a compressed air energy storage system. Renewable energy, 83, pp.491-509.

Avanessian, T. and Ameri, M., 2014. Energy, exergy, and economic analysis of single and double effect LiBr–H_2O absorption chillers. Energy and Buildings, 73, pp.26-36.

Budt, M., Wolf, D., Span, R. and Yan, J., 2016. A review on compressed air energy storage: Basic principles, past milestones and recent developments. Applied energy, 170, pp.250-268.

Cazzaniga, R., Cicu, M., Rosa-Clot, M., Rosa-Clot, P., Tina, G.M. and Ventura, C., 2017. Compressed air energy storage integrated with floating photovoltaic plant. Journal of Energy Storage, 13, pp.48-57.

Chai, Y., Gao, N., Wang, M. and Wu, C., 2020. H2 production from co-pyrolysis/gasification of waste plastics and biomass under novel catalyst Ni-CaO-

574 C. Chemical Engineering Journal, 382, p.122947.
575 Chen, H., Cong, T.N., Yang, W., Tan, C., Li, Y. and Ding, Y., 2009. Progress in
576 electrical energy storage system: A critical review. Progress in natural science, 19(3),
577 pp.291-312.
578 Chen, W., Shi, C., Zhang, S., Chen, H., Chong, D. and Yan, J., 2017. Theoretical
579 analysis of ejector refrigeration system performance under overall modes. Applied
580 Energy, 185, pp.2074-2084.
581 Canepa, R., Wang, M., Biliyok, C. and Satta, A., 2013. Thermodynamic analysis of
582 combined cycle gas turbine power plant with post-combustion CO2 capture and exhaust
583 gas recirculation. Proceedings of the Institution of Mechanical Engineers, Part E:
584 Journal of Process Mechanical Engineering, 227(2), pp.89-105.
585 Cavallo, A., 2007. Controllable and affordable utility-scale electricity from
586 intermittent wind resources and compressed air energy storage (CAES). Energy, 32(2),
587 pp.120-127.
588 Crotogino, F., Mohmeyer, K.U. and Scharf, R., 2001, April. Huntorf CAES: More
589 than 20 years of successful operation. In SMRI Spring meeting (Vol. 2001).
590 Gomri, R., 2009. Second law comparison of single effect and double effect vapour
591 absorption refrigeration systems. Energy Conversion and Management, 50(5), pp.1279-
592 1287.
593 He, F., Xu, Y., Zhang, X., Liu, C. and Chen, H., 2015. Hybrid CCHP system
594 combined with compressed air energy storage. International Journal of Energy
595 Research, 39(13), pp.1807-1818.
596 Herold, K.E., Radermacher, R. and Klein, S.A., 2016. Absorption chillers and heat
597 pumps. CRC press.
598 IEA. 2020. Renewables 2020 – Analysis - IEA. [online] Available at:

599 <https://www.iea.org/reports/renewables-2020> [Accessed 29 November 2020].
600 Jafarizadeh, H., Soltani, M. and Nathwani, J., 2020. Assessment of the Huntorf
601 compressed air energy storage plant performance under enhanced modifications.
602 Energy Conversion and Management, 209, p.112662.
603 Kheiri, R. and Ghaebi, H., 2017. Thermodynamic modeling of a novel and modified
604 Organic Rankine Cycle (ORC) augmented with ejector and regenerator. Modares
605 Mechanical Engineering, 16(13), pp.23-27.
606 Kousksou, T., Bruel, P., Jamil, A., El Rhafiki, T. and Zeraouli, Y., 2014. Energy
607 storage: Applications and challenges. Solar Energy Materials and Solar Cells, 120,
608 pp.59-80.
609 Krupke, C., Wang, J., Clarke, J. and Luo, X., 2016. Modeling and experimental study
610 of a wind turbine system in hybrid connection with compressed air energy
611 storage. IEEE Transactions on Energy Conversion, 32(1), pp.137-145.
612 McNevin, C. and Harrison, S.J., 2017. Multi-stage liquid-desiccant air-conditioner:
613 Experimental performance and model development. Building and Environment, 114,
614 pp.45-55.
615 Meng, H., Wang, M., Aneke, M., Luo, X., Olumayegun, O. and Liu, X., 2018.
616 Technical performance analysis and economic evaluation of a compressed air energy
617 storage system integrated with an organic Rankine cycle. Fuel, 211, pp.318-330.
618 Meng, H., Wang, M., Olumayegun, O., Luo, X. and Liu, X., 2019. Process design,
619 operation and economic evaluation of compressed air energy storage (CAES) for wind
620 power through modelling and simulation. Renewable energy, 136, pp.923-936.
621 Misra, R.D., Sahoo, P.K., Sahoo, S. and Gupta, A., 2003. Thermoeconomic
622 optimisation of a single effect water/LiBr vapour absorption refrigeration system.
623 International Journal of refrigeration, 26(2), pp.158-169.

624 Mohammadi, A., Ahmadi, M.H., Bidi, M., Joda, F., Valero, A. and Uson, S., 2017.
625 Exergy analysis of a Combined Cooling, Heating and Power system integrated with
626 wind turbine and compressed air energy storage system. Energy Conversion and
627 Management, 131, pp.69-78.
628 Letcher, T.M. ed., 2020. Future energy: improved, sustainable and clean options for
629 our planet. Elsevier.
630 Luo, X., Wang, J., Dooner, M. and Clarke, J., 2015. Overview of current
631 development in electrical energy storage technologies and the application potential in
632 power system operation. Applied energy, 137, pp.511-536.
633 Quoilin, S., Van Den Broek, M., Declaye, S., Dewallef, P. and Lemort, V., 2013.
634 Techno-economic survey of Organic Rankine Cycle (ORC) systems. Renewable and
635 Sustainable Energy Reviews, 22, pp.168-186.
636 Radgen, P., 2008, November. Years Compressed Air Energy Storage Plant
637 Huntorf—Experiences and Outlook. In Proceedings of the 3rd International Renewable
638 Energy Storage Conference, Berlin, Germany (pp. 24-25).
639 Sadreddini, A., Fani, M., Aghdam, M.A. and Mohammadi, A., 2018. Exergy analysis
640 and optimisation of a CCHP system composed of compressed air energy storage system
641 and ORC cycle. Energy conversion and management, 157, pp.111-122.
642 Sioshansi, R., Denholm, P. and Jenkin, T., 2011. A comparative analysis of the value
643 of pure and hybrid electricity storage. Energy Economics, 33(1), pp.56-66.
644 Simpore S., Garde, F. David, M. Marc O. and Castaing-Lasvignottes J., 2016. Design
645 and dynamic simulation of a compressed air energy storage system (CAES) coupled
646 with a building, an electric grid and photovoltaic power plant. CLIMA 2016, Aalborg,
647 Denmark (2016)
648 Soltani, M., Nabat, M.H., Razmi, A.R., Dusseault, M.B. and Nathwani, J., 2020. A

649 comparative study between ORC and Kalina based waste heat recovery cycles applied
650 to a green compressed air energy storage (CAES) system. Energy Conversion and
651 Management, 222, p.113203.
652 Somers, C., Mortazavi, A., Hwang, Y., Radermacher, R., Rodgers, P. and Al-
653 Hashimi, S., 2011. Modeling water/lithium bromide absorption chillers in ASPEN Plus.
654 Applied Energy, 88(11), pp.4197-4205.
655 Souza, R.J., Dos Santos, C.A.C., Ochoa, A.A.V., Marques, A.S., Neto, J.L.M. and
656 Michima, P.S.A., 2020. Proposal and 3E (energy, exergy, and exergoeconomic)
657 assessment of a cogeneration system using an organic Rankine cycle and an Absorption
658 Refrigeration System in the Northeast Brazil: Thermodynamic investigation of a
659 facility case study. Energy conversion and Management, 217, p.113002.
660 Wang, J., Yan, Z., Wang, M., Ma, S. and Dai, Y., 2013. Thermodynamic analysis
661 and optimisation of an (organic Rankine cycle) ORC using low grade heat source.
662 Energy, 49, pp.356-365.
663 Yan, Y., Zhang, C., Li, K. and Wang, Z., 2018. An integrated design for hybrid
664 combined cooling, heating and power system with compressed air energy
665 storage. Applied Energy, 210, pp.1151-1166.
666 Yao, E., Wang, H., Wang, L., Xi, G. and Maréchal, F., 2016. Thermo-economic
667 optimisation of a combined cooling, heating and power system based on small-scale
668 compressed air energy storage. Energy Conversion and Management, 118, pp.377-386.
669 Zhang, Y., Yang, K., Li, X. and Xu, J., 2014. Thermodynamic analysis of energy
670 conversion and transfer in hybrid system consisting of wind turbine and advanced
671 adiabatic compressed air energy storage. Energy, 77, pp.460-477.
672 Zhang, Y., Xu, Y., Zhou, X., Guo, H., Zhang, X. and Chen, H., 2017. Compressed
673 air energy storage system with variable configuration for wind power

674 generation. Energy Procedia, 142, pp.3356-3362.
675 Zhao, P., Dai, Y. and Wang, J., 2015. Performance assessment and optimization of a
676 combined heat and power system based on compressed air energy storage system and
677 humid air turbine cycle. Energy Conversion and Management, 103, pp.562-572.
678 Zhao, P., Gao, L., Wang, J. and Dai, Y., 2016. Energy efficiency analysis and off-
679 design analysis of two different discharge modes for compressed air energy storage
680 system using axial turbines. Renewable energy, 85, pp.1164-1177.
681 Zhou, Q., Du, D., Lu, C., He, Q. and Liu, W., 2019. A review of thermal energy
682 storage in compressed air energy storage system. Energy, 188, p.115993.
683